

Mass-independent test of quantumness of a massive object

Debarshi Das,^{1,*} Dipankar Home,² Hendrik Ulbricht,³ and Sougato Bose¹

¹*Department of Physics and Astronomy, University College London,
Gower Street, London WC1E 6BT, England, United Kingdom*

²*Center for Astroparticle Physics and Space Science (CAPSS), Bose Institute, Kolkata 700 091, India*

³*School of Physics and Astronomy, University of Southampton, Southampton SO17 1BJ, England, United Kingdom*

Search for empirically implementable schemes that can evidence the nonclassicality of large masses is a quest currently attracting considerable research. Motivated by this, we investigate the quantum violation of the pivotal classical notion of macrorealism (MR) for arbitrary masses in a harmonic potential. To this end, we use two standard tools for probing the violation of MR, namely the two-time Leggett-Garg inequality (LGI) and the no-signalling in time (NSIT) condition, but crucially, modify them to the case of two different measurement arrangements at successive times. This yields a striking result: a *mass-independent* violation of MR is possible, thereby providing a mass-independent demonstration of an irreducible quantumness of macroscopic objects. In fact, our adaptation of LGI and NSIT enables probing quantum violations for literally any mass, momentum, energy and frequency. Our proposed test of MR can in principle be realised with a large range of harmonic oscillator systems from atomic ions to mirrors in LIGO, while the uncertainties in the measurements for large masses can be offset by decreasing the angular frequency, suggesting that for such systems MR test can be performed based on existing experimental technology.

Introduction and motivation:— A cutting-edge research enterprise in contemporary physics is to explore realizable schemes towards empirically checking the validity of the quantum mechanical (QM) principle of superposition of states in the macroscopic regime, together with demonstrating its incompatibility with the world view based on the classical notion of macrorealism (MR) [1]. The goal is to expand as much possible the macroscopic domain of such testability. This has also potentiality in providing useful empirical constraints on suggested modifications of quantum dynamical evolution in the macroscopic limit (such as the models of spontaneous wave function collapse [2–4]), which suppress superposition of states at the macrolevel. Nonclassical massive matter states are also a resource for nonclassical gravity [5–10]. An important challenge is, however, to test MR (and through it, nonclassicality) even *without* preparing nonclassical states.

The key tools for probing MR are “temporal correlators” from which one constructs the Leggett-Garg inequalities (LGI) [11] and the no-signalling in time (NSIT) conditions [12]. Such relations are derived from a conjunction of the following assumptions, as formulated by Leggett and Garg [11, 13]: (i) At any instant, even if unobserved, a system is definitely in one of its possible states with all its observable properties having definite values (realism per se). (ii) It is possible to determine which of the states the system is in by ensuring the measurement-induced disturbance to be arbitrarily small, thus not affecting the subsequent time evolution of the measured state of the system (noninvasive measurability). (iii) The outcome of a measurement is not affected by what will be measured subsequently (induction). An experimental refutation of MR embodying these assumptions, in accordance with the QM predictions, would constitute a decisive evidence of macroscopic nonclassicality, together with certifying the validity of QM principle of superposition of states at the macrolevel.

With growing interest on this fundamentally significant topic, particularly over the past two decades, a number of experimental studies seeking to test MR have been reported (for a useful review of the earlier experiments, see Ref. [14]). Among the experiments in the recent years, the following ones need to be specially noted: (a) Violation of LGI has been shown using neutrino flavour oscillations [15] where the relevant “macroscopicity” measure is the length scale of neutrino oscillation of about 735 km over which the LGI violation has been found. (b) In the experiment involving a superconducting flux qubit [16], the relevant “macroscopicity” measure is taken to be the difference of the magnetic moments corresponding to the two superposing superconducting current states (each of 170 nA current); this difference is of the order of 10^4 Bohr magneton, and the empirical violation of MR is shown using a suitable NSIT condition. (c) In a very recent interferometric experiment based on heralded single photons [17], loophole-free violations of both LGI and its variant [18] have been demonstrated, where the “macroscopicity” measure is of the order of 10^4 , specifying the extent to which the spatial separation between the two superposing single photon states (corresponding to the two arms of the interferometer) is larger than the photonic wavelength of 810 nm used in this experiment.

It should therefore be clear from the preceding discussion that the figure of merit used to characterise “macroscopicity” is crucially dependent on the experimental specifics. A variety of “macroscopicity” measures have been invoked for testing MR in different contexts. However, while ‘mass’ seems to be a quite relevant parameter for characterising “macroscopicity”, *no experiment testing MR has yet been performed based on systems having significantly large mass* - a few earlier LGI based experiments employing atomic systems have been confined to using, for example, a single cesium atom [19] and spin-bearing phosphorus impurities in silicon [20]. On the other hand, the tests of quantumness per se of macromolecules (without seeking to test MR) have yet reached only up to masses about 10^4 amu [21, 22]. Our present work is motivated

* debarshi.das@ucl.ac.uk

towards *filling this important gap* in the relevant literature by formulating a suitable scheme that can enable scaling up the test of MR vis-à-vis QM to arbitrarily large masses.

Towards this end, we introduce a suitable variation in the testing procedures based on the LGI and the NSIT relation in the context of a harmonically oscillating object in a minimum-uncertainty Gaussian nonspreading wave packet whose peak follows classical dynamics. There have been earlier analyses of QM violations of MR for coherent states [23, 24]. However, these violations happened for a narrow parameter domain, thereby restricting its realizability with large masses. In contrast, here we find, by an appropriate modification of the LGI/NSIT procedure, that a *mass independent* QM violation of MR is possible. In fact, for literally *any* choice of parameters – mass, energy, frequency, our procedure can certify macroscopic quantumness and show violation of MR.

The basic ideas of our scheme:– Let us begin by noting that the various versions of macrorealist inequalities/conditions that have been applied in different contexts usually consider the same observable to be successively measured on a single particle evolving in time. In contrast, here for the example considered, the successive measurements are invoked in such a way that they pertain to different observables. Let us now explain how this is realised. For a one-dimensional system harmonically oscillating between $x = -\infty$ to $x = \infty$, dividing this domain of oscillation into two sub-domains, ranging from $x = -\infty$ to $x = \beta_i$ and $x = \beta_i$ to $x = \infty$, where β_i is any real number, we consider coarse-grained spatial measurement at an instant $t = t_i$ that determines which one of these two regions the oscillating system is in at the given instant. A key element of our scheme is that the location $x = \beta_i$ of the boundary between the two regions for the type of measurement considered is chosen according to the instant $t = t_i$ at which the measurement is made. For convenience, considering that the initial coherent state Gaussian wave function at $t = 0$ is peaked at $x = 0$, we choose the instant of the first measurement at the initial instant, i.e., $t_1 = 0$ and the boundary for this measurement to be located at $x = \beta_1 = 0$.

Next, for the subsequent measurement at the instant $t = t_2$, the appropriate choice of the location $x = \beta_2$ of the boundary between the two measurement regions is critical in order to achieve the desired mass-independence of the quantum violation of MR. Towards attaining this goal, our analysis reveals that by suitably fixing β_2 for given values of t_2 , it is possible to ensure the magnitudes of the quantum violations of both the two-time LGI [25] and the two-time NSIT relation [12, 18] to be independent of mass, as well as of the other relevant experimental parameters such as the initial peak momentum and the angular frequency. Here it needs to be pointed out that if the observable quantity is taken to be such that at any instant, it takes a value +1 (–1) depending on whether the system is in one region or in the other, it is then evident that in this example, such an observable quantity changes according to the location of the boundary demarcating the two measurement regions. Hence, for the purpose of the following analysis, the two-time LGI and the two-time NSIT relation invoked are, crucially, in terms of different observable quantities being measured at two different instants. Here note that the deriva-

tions of LGI and NSIT relations from MR do not depend upon the measured quantity to be necessarily the same at the different instants of successive measurements.

A couple of further relevant points also require to be mentioned here. First, it is operationally advantageous to test two-time macrorealist relations compared to the three-time ones because of the lesser number of joint probabilities measured. Among the two-time macrorealist relations, the NSIT condition involves minimum number of observable probabilities. Secondly, the measurement envisaged in our example can be designed such that an outcome is inferred when the detector is not triggered (negative result measurement). This ensures that there is no classical interaction with the measured object during measurement, thereby satisfying the assumption of noninvasive measurability [13]. Such a measurement can be implemented in our setup by using, say, a probe beam for illuminating one of the two regions (either from $x = \beta_i$ to $x = \infty$, or from $x = \beta_i$ to $x = -\infty$). If no scattered light is observed, an outcome is registered by inferring the presence of the oscillating object within the unilluminated region [23]. Other relevant specifics will be discussed with respect to the analysis of our scheme presented as follows.

The analysis:– We begin by explicitly writing the modified forms of the two-time LGI and the two-time NSIT relation involving sequential measurements of the observables denoted by Q and R at two different instants $t = t_1$ and $t = t_2$ respectively, where $t_1 < t_2$. The NSIT condition implies that the probability of obtaining a particular outcome for the measurement of R at $t = t_2$ should be independent of whether any prior measurement has been carried out. That is, in the present context, the two-time NSIT condition can be expressed as

$$N_{\pm} = p(R_{\pm}) - [p(Q+, R_{\pm}) + p(Q-, R_{\pm})] = 0. \quad (1)$$

where $p(Q+, R+)$ is the joint probability of getting the outcomes +1 at instant $t = t_1$ and +1 at instant $t = t_2$, similarly, for other joint probabilities. On the other hand, $p(R+)$ is the probability of getting the outcome +1 at instant $t = t_2$, when no measurement is done at $t = t_1$, similarly, for $p(R-)$. Magnitude of quantum violation of the two-time NSIT condition will be denoted by the non-zero value of $|N_{\pm}|$.

In this scenario, the two-time LGI can be expressed as (see Appendix A for the derivation)

$$L_{s_1, s_2} = 1 + s_1 \langle Q \rangle + s_2 \langle R \rangle + s_1 s_2 \langle QR \rangle \geq 0, \\ \text{with } s_1, s_2 \in \{+1, -1\}, \quad (2)$$

where the correlation function $\langle QR \rangle = p(Q+, R+) - p(Q+, R-) - p(Q-, R+) + p(Q-, R-)$; and the expectation values $\langle Q \rangle = p(Q+) - p(Q-)$, $\langle R \rangle = p(R+) - p(R-)$. Here $\langle R \rangle$ is defined when no measurement at $t = t_1$ is performed. In this case, magnitude of quantum violation of the two-time LGI will be denoted by the positive value of $\max_{s_1 = \pm 1, s_2 = \pm 1} (-L_{s_1, s_2})$.

Consider the following initial Gaussian wave function of the coherent state peaked at $x = 0$ at instant $t = 0$,

$$\psi(x, t = 0) = \sqrt{\frac{1}{\sqrt{2\pi}\sigma_0}} \exp\left(-\frac{x^2}{4\sigma_0^2} + \frac{ip_0 x}{\hbar}\right) \quad (3)$$

with the initial momentum expectation value p_0 , and the width $\sigma_0 = \sqrt{\hbar/(2m\omega)}$, where ω is the angular frequency of oscillation and m is the mass. The time evolution of this state is evaluated in this example using linear harmonic oscillator potential.

We consider measurements of Q and R at the instants $t = t_1$ and $t = t_2$ respectively, where Q and R correspond to the earlier mentioned coarse-grained measurements. To put it specifically, Q is an observable quantity such that it takes a value $+1$ (-1) depending on whether the system is in the region from $x = \beta_1$ to $x = \infty$ (from $x = -\infty$ to $x = \beta_1$). Similarly, R is another observable quantity such that it takes a value $+1$ (-1) if the particle is in the region from $x = \beta_2$ to $x = \infty$ (from $x = -\infty$ to $x = \beta_2$). Such a coarse-grained position measurement at instant $t = t_i$ ($i = 1, 2$) can be represented by the operator $\hat{O}_i = \int_{\beta_i}^{\infty} |x\rangle\langle x| dx - \int_{-\infty}^{\beta_i} |x\rangle\langle x| dx$, which has two eigenvalues $+1$ and -1 .

As mentioned earlier, $\beta_1 = 0$. With this choice of β_1 , it can be shown that the expressions for the joint probabilities are the following functions of β_2 and other relevant parameters given by,

$$p(Q\pm, R-) = \frac{1}{4\sqrt{\pi}} \int_{-\infty}^{\gamma} dx \exp[-x^2] f(x, \omega t_2),$$

$$p(Q\pm, R+) = \frac{1}{4\sqrt{\pi}} \int_{\gamma}^{\infty} dx \exp[-x^2] f(x, \omega t_2), \quad (4)$$

$$\text{with } f(x, \omega t_2) = \left| 1 \pm \text{erf} \left[\frac{-ix}{\sin(\omega t_2) \sqrt{2 - 2i \cot(\omega t_2)}} \right] \right|^2, \quad (5)$$

$$\text{and } \gamma = \beta_2 \sqrt{\frac{m\omega}{\hbar}} - \frac{p_0 \sin(\omega t_2)}{\sqrt{\hbar m \omega}}, \quad (6)$$

where the error function $\text{erf}(z) = (2/\sqrt{\pi}) \int_0^z dt \exp(-t^2)$. Similarly, we have the following form of probabilities,

$$p(Q\pm) = \frac{1}{2}; \quad p(R\pm) = \frac{1}{2} [1 \mp \text{erf}(\gamma)]. \quad (7)$$

The details of these calculations are given in Appendix B.

Next, we have to choose β_2 suitably for the measurement at $t = t_2$. Our heuristic arguments based on physical ground (see Appendix C) suggest that the location of the peak at the instant $t = t_2$, given by $x_0^{(t_2)} = p_0 \sin(\omega t_2)/(m\omega)$, together with the standard deviation $\Delta^{(t_2)} = \sqrt{\hbar/(2m\omega)}$ of the probability density without any prior measurement at $t = t_1$ would play critical role in fixing β_2 suitably for our purpose. Guided by this consideration, our in-depth investigation reveals that if the choice of β_2 is made at $x_0^{(t_2)} \pm c\Delta^{(t_2)}$ with $c > 0$ being of the order of 10^{-1} or 1, the possibility indeed arises for obtaining quantum violations of both the two-time NSIT condition and the two-time LGI. Here a key point is that this choice of $\beta_2 = x_0^{(t_2)} \pm c\Delta^{(t_2)}$ leads to γ given by Eq.(6) becoming independent of m , ω and p_0 , i.e., γ is then determined by only the chosen value of c , whence $\gamma = \pm c/\sqrt{2}$. Consequently, the probability distributions (4) and (7) become functions of (ωt_2) only. This, therefore, enables the quantum violations of

m	p_0	ω	t_2	Magnitude of Quantum Violation of two-time NSIT: $ N_{\pm} $	Magnitude of Quantum Violation of two-time LGI: $\max_{s_1=\pm 1, s_2=\pm 1} (-L_{s_1, s_2})$
Any	Any	Any	$\frac{T}{14}$	0.12	0.08
Any	Any	Any	$\frac{T}{8}$	0.15	0.04
Any	Any	Any	$\frac{T}{4}$	0.17	No Violation
Any	Any	Any	$\frac{T}{3}$	0.16	No Violation
Any	Any	Any	$\frac{3T}{8}$	0.15	0.04
Any	Any	Any	$\frac{2T}{5}$	0.14	0.07
Any	Any	Any	$\frac{3T}{4}$	0.17	No Violation

TABLE I: Quantum violations of the two-time no-signalling in time (NSIT) condition and the two-time Leggett-Garg inequalities (LGI) when the boundary between the two regions in case of the second measurement is chosen to be located at $x = \beta_2 = p_0 \sin(\omega t_2)/(m\omega) + \sqrt{\hbar/(m\omega)}$. Here $T = 2\pi/\omega$ denotes the time period.

the two-time NSIT condition and the two-time LGI to become independent of mass. That it is indeed the case is confirmed comprehensively by evaluating numerically the integrations appearing in (4). In Table I, some illustrative results are presented by choosing, for example, $c = \sqrt{2}$. These results indicate and is confirmed by detailed study that the two-time NSIT condition is violated for a wider range of choices of t_2 than that for the two-time LGI. To sum up, the upshot of this entire study is that it is always, in principle, possible to choose t_2 suitably depending on the time period of the oscillating particle to obtain quantum violation of the two-time NSIT condition or the two-time LGI for any m , p_0 and ω .

Practical challenges with large mass:— Ideally, in our scheme, one of the two regions (either from $x = -\infty$ to $x = \beta_i$ or from $x = \beta_i$ to $x = \infty$) should be illuminated at an instant $t = t_i$. In practice, however, it is almost impossible to keep the boundary between the two regions (illuminated and unilluminated) fixed in all experimental runs. Rather, we can expect that the aforementioned boundary at $t = t_i$ will be at $x = \beta_i + \epsilon_i$ (with ϵ_i being a small positive/negative number depending on the accuracy of the experimental setup), where ϵ_i will be different in different runs. In effect, the observed violation of the two-time NSIT condition will be the statistical average over different values of N_+ , N_- corresponding to different values of ϵ_1 and ϵ_2 . Similar will be the case for the two-time LGI. It can be shown that the permissible ranges of ϵ_1 and ϵ_2 to get significant violation of the two-time NSIT or the two-time LGI are proportional to $1/\sqrt{m\omega}$ (details are presented in Appendix D). Hence, the required precision in fixing the boundary between the two measurement regions at any instant is increased with increasing mass. Nonetheless, the effect of increasing mass in this context can be offset by decreasing the angular frequency ω . Here, it is relevant to note that the lowest angular frequency of a harmonic well achieved till date is $\omega \sim 100$ kHz in case of optical trap [26], $\omega \sim 100$ Hz in case of ion trap [27, 28] and 1 – 10 Hz in

diamagnetic trap [29, 30]. For small ω , the violations as mentioned in Table I are observed for large t_2 . For any ω , damping has to be controlled so that the decoherence rate due to all force noises given by $\gamma = S_{FF}(\omega)(\Delta x)^2/\hbar^2 \ll 1/t_2$, where $S_{FF}(\omega)$ is the noise power density of force and Δx is the width of the wave-function at t_2 . Since both *with or without* measurement at t_1 , $\Delta x \sim \sigma_0 = \sqrt{\hbar/(2m\omega)}$ (see Fig. 1 and Fig. 2 in Appendix C), the above condition reduces to $\sqrt{S_{FF}(\omega)} \ll \omega\sqrt{\hbar m}/\sqrt{\pi}$ for $t_2 \sim T$. Interestingly, large masses indeed help here, for the obvious reason that force noise induces less random acceleration.

Possible experimental implementations:— We can envisage implementations with nano and micro-objects (typically up to $\sim 10^{-14}$ kg) based on so-called levitated mechanics [31] in various low-noise traps such as optical dipole traps, ion traps, magnetic and diamagnetic traps in vacuum and at low temperature, but also using much larger masses (~ 10 kg) in the gravitational wave detectors [32]. We consider making use of the mass-independency of this MR test in choosing experimental setups optimised to reduce relevant decoherence effects, noises, as well as for addressing at the same time the need for high spatial detection resolution of the centre of mass motion of the trapped particle. The preparation of the initial state will be accomplished by cooling, for instance by feedback [33], to a motional state of low occupation number, for which the only requirement is that the rate of acquiring information about the object is much faster than the rate of its heating from environmental noise [34–36]. This technique has already been used for cooling to the ground state for $\omega \sim 100$ kHz traps [37, 38] as well as for a large mass and low frequency ($\omega \sim 100$ Hz) gravitational wave detector [32]. The conditions are well within ultra-high vacuum at 10^{-10} mbar and can be done in low temperature environments even below 10 mK and with vibration isolation. We consider the high efficiency and high spatial resolution of detection the most severe challenge for a realisation of this MR scheme, similar as for measurement-based state manipulation schemes [39, 40].

However, we believe there is a possibility for the realisation of this experiment in principle, for example in an optical detection scenario, if we are using the detection of scattered light from the particle to detect its motion, for an assumed near-unity efficiency of collection of the scattered light, and for n photons, we obtain a resolution of λ/\sqrt{n} with $\lambda \sim \mu\text{m}$. This implies the collection of $n \sim 10^8$ photons for reaching a spatial resolution of the ground state spread σ_0 of a $m \sim 10^{-14}$ kg particle in a $\omega \sim 1$ Hz trap. If the scattered power is nW this information is acquired in $\sim 10^{-2}$ s, implying that all other heating rates, such as by interactions with black-body photons and by gas collisions have to be at $\Gamma \leq 10^2$ Hz ($\Gamma \sim \mu\text{Hz}$ has already been achieved [41]).

For increasing the critical detection efficiency in light scattering techniques one could use collection optics with high numerical aperture, for example, parabolic mirrors [42]. The high spatial resolution could be achieved by illuminating only either to the left or right of $x = \beta_i$ at instant $t = t_i$ with a sharp profile of drop at the point $x = \beta_i$. If after 0.01 s with a nW laser, no scattered light is obtained, it immediately implies that the operator having acted upon the object, for light shown on the left half, is the projector associated with the +1 eigenvalue of \hat{O}_i with the location of the boundary between the two measurement regions, $x = \beta_i$, being at angstrom resolution. Such spatial resolution has been achieved in optical imaging of single molecules [43] and indeed optomechanical experiments [36, 44] by using optical interferometry.

Conclusions:— We have suitably modified the procedure for testing LGI and NSIT in order to show the violation of the classical notion of MR in a manner which is *independent* of the parameters: mass, energy, frequency. Naturally, this enormously broadens the scope for evidencing non-classicality for large masses. No nonclassical state, such as a quantum superposition of distinct states (e.g., a Schrödinger cat state) or even a squeezed state, needs to be prepared a priori. Moreover, this approach does not require coupling with any ancillary quantum system or using nonlinearity. Rather the starting point of our scheme is the most “classical-like” of all quantum states, namely the coherent state which has been prepared by feedback cooling in several systems [33], including 10 kg LIGO masses [32], and imminent in several other systems. We have shown that merely coarse-grained spatial measurements on such feedback cooled systems can witness their intrinsic non-classicality, irrespective of their mass and energy.

Acknowledgements:— We acknowledge fruitful discussions with Jonathan Halliwell and Clement Mawby. DD acknowledges the Royal Society (United Kingdom) for the support through the Newton International Fellowship (NIF\R1\212007). DH acknowledges support from NASI Senior Scientist Fellowship and QuEST-DST Project Q-98 of the Government of India. HU would like to acknowledge support EPSRC through grants EP/W007444/1, EP/V035975/1 and EP/V000624/1, the Leverhulme Trust (RPG-2022-57), the EU Horizon 2020 FET-Open project TeQ (766900), and the EU EIC Pathfinder project QuCoM (10032223). SB would like to acknowledge EPSRC grants (EP/N031105/1 and EP/S000267/1) and grant ST/W006227/1.

Note Added:— We are aware that a related paper by an independent group, reporting the latest most elaborate and rigorous study of QM violations of the different forms of LGI for Gaussian states seeking to maximize the magnitudes of these violations is appearing in parallel [45].

-
- [1] A. J. Leggett, *Testing the limits of quantum mechanics: motivation, state of play, prospects*, *J. Phys. Condens. Matter* **14**, R415 (2002).
 [2] G. C. Ghirardi, A. Rimini, and T. Weber, *Unified dynamics for microscopic and macroscopic systems*, *Phys. Rev. D* **34**, 470

- (1986).
 [3] P. Pearle, *Combining stochastic dynamical state-vector reduction with spontaneous localization*, *Phys. Rev. A* **39**, 2277 (1989).
 [4] A. Bassi, K. Lochan, S. Satin, T. P. Singh, and H. Ulbricht,

- Models of wave-function collapse, underlying theories, and experimental tests*, *Rev. Mod. Phys.* **85**, 471 (2013).
- [5] S. Bose, A. Mazumdar, G. W. Morley, H. Ulbricht, M. Toros, M. Paternostro, A. A. Geraci, P. F. Barker, M. S. Kim, and G. Milburn, *Spin Entanglement Witness for Quantum Gravity*, *Phys. Rev. Lett.* **119**, 240401 (2017).
- [6] C. Marletto, and V. Vedral, *Gravitationally Induced Entanglement between Two Massive Particles is Sufficient Evidence of Quantum Effects in Gravity*, *Phys. Rev. Lett.* **119**, 240402 (2017).
- [7] R. J. Marshman, A. Mazumdar, and S. Bose, *Locality and entanglement in table-top testing of the quantum nature of linearized gravity*, *Phys. Rev. A* **101**, 052110 (2020).
- [8] S. Bose, A. Mazumdar, M. Schut, and M. Toros, *Mechanism for the quantum natured gravitons to entangle masses*, *Phys. Rev. D* **105**, 106028 (2022).
- [9] M. Christodoulou, and C. Rovelli, *On the possibility of laboratory evidence for quantum superposition of geometries*, *Phys. Lett. B* **792**, 64 (2019).
- [10] M. Christodoulou, A. D. Biagio, M. Aspelmeyer, C. Brukner, C. Rovelli, and R. Howl, *Locally mediated entanglement through gravity from first principles*, [arXiv:2202.03368 \[quant-ph\]](https://arxiv.org/abs/2202.03368).
- [11] A. J. Leggett and A. Garg, *Quantum mechanics versus macroscopic realism: Is the flux there when nobody looks?*, *Phys. Rev. Lett.* **54**, 857 (1985).
- [12] J. Kofler and C. Brukner, *Condition for macroscopic realism beyond the Leggett-Garg inequalities*, *Phys. Rev. A* **87**, 052115 (2013).
- [13] A. J. Leggett, *Realism and the physical world*, *Rep. Prog. Phys.* **71**, 022001 (2008).
- [14] C. Emary, N. Lambert, and F. Nori, *Leggett–Garg inequalities*, *Rep. Prog. Phys.* **77**, 016001 (2014).
- [15] J. A. Formaggio, D. I. Kaiser, M. M. Murskyj, and T. E. Weiss, *Violation of the Leggett–Garg Inequality in Neutrino Oscillations*, *Phys. Rev. Lett.* **117**, 050402 (2016).
- [16] G. C. Knee, K. Kakuyanagi, M.-C. Yeh, Y. Matsuzaki, H. Toida, H. Yamaguchi, S. Saito, A. J. Leggett, and W. J. Munro, *A strict experimental test of macroscopic realism in a superconducting flux qubit*, *Nat. Commun.* **7**, 13253 (2016).
- [17] K. Joarder, D. Saha, D. Home, and U. Sinha, *Loophole-Free Interferometric Test of Macrorealism Using Heralded Single Photons*, *PRX Quantum* **3**, 010307 (2022).
- [18] D. Saha, S. Mal, P. K. Panigrahi, and D. Home, *Wigner’s form of the Leggett-Garg inequality, the no-signaling-in-time condition, and unsharp measurements*, *Phys. Rev. A* **91**, 032117 (2015).
- [19] C. Robens, W. Alt, D. Meschede, C. Emary, and A. Alberti, *Ideal Negative Measurements in Quantum Walks Disprove Theories Based on Classical Trajectories*, *Phys. Rev. X* **5**, 011003 (2015).
- [20] G. C. Knee, S. Simmons, E. M. Gauger, J. J. Morton, H. Riemann, N. V. Abrosimov, P. Becker, H.-J. Pohl, K. M. Itoh, M. L. Thewalt, G. A. D. Briggs, and S. C. Benjamin, *Violation of a Leggett–Garg inequality with ideal non-invasive measurements*, *Nat. Commun.* **3**, 606 (2012).
- [21] S. Gerlich, S. Eibenberger, M. Tomandl, S. Nimmrichter, K. Hornberger, P. J. Fagan, J. Tüxen, M. Mayor, and M. Arndt, *Quantum interference of large organic molecules*, *Nat Commun* **2**, 263 (2011).
- [22] Y. Y. Fein, P. Geyer, P. Zwick, F. Kialka, S. Pedalino, M. Mayor, S. Gerlich, and M. Arndt, *Quantum superposition of molecules beyond 25 kDa*, *Nat. Phys.* **15**, 1242 (2019).
- [23] S. Bose, D. Home, and S. Mal, *Nonclassicality of the Harmonic-Oscillator Coherent State Persisting up to the Macroscopic Domain*, *Phys. Rev. Lett.* **120**, 210402 (2018).
- [24] J. J. Halliwell, A. Bhatnagar, E. Ireland, H. Nadeem, and V. Wimalaweera, *Leggett-Garg tests for macrorealism: Interference experiments and the simple harmonic oscillator*, *Phys. Rev. A* **103**, 032218 (2021).
- [25] J. J. Halliwell, *Leggett-Garg inequalities and no-signaling in time: A quasiprobability approach*, *Phys. Rev. A* **93**, 022123 (2016).
- [26] J. Bateman, S. Nimmrichter, K. Hornberger, and H. Ulbricht, *Near-field interferometry of a free-falling nanoparticle from a point-like source*, *Nat. Commun.* **5**, 4788 (2014).
- [27] P. Z. G. Fonseca, E. B. Aranas, J. Millen, T. S. Monteiro, and P. F. Barker, *Nonlinear Dynamics and Strong Cavity Cooling of Levitated Nanoparticles*, *Phys. Rev. Lett.* **117**, 173602 (2016).
- [28] J. Millen, P. Z. G. Fonseca, T. Mavrogordatos, T. S. Monteiro, and P. F. Barker, *Cavity Cooling a Single Charged Levitated Nanosphere*, *Phys. Rev. Lett.* **114**, 123602 (2015).
- [29] Y. Leng, R. Li, X. Kong, H. Xie, D. Zheng, P. Yin, F. Xiong, T. Wu, C.-K. Duan, Y. Du, Z.-q. Yin, P. Huang, and J. Du, *Mechanical Dissipation Below 1 μ Hz with a Cryogenic Diamagnetic Levitated Micro-Oscillator*, *Phys. Rev. Applied* **15**, 024061 (2021).
- [30] D. Zheng, Y. Leng, X. Kong, R. Li, Z. Wang, X. Luo, J. Zhao, C.-K. Duan, P. Huang, J. Du, M. Carlesso, and A. Bassi, *Room temperature test of the continuous spontaneous localization model using a levitated micro-oscillator*, *Phys. Rev. Research* **2**, 013057 (2020).
- [31] C. Gonzalez-Ballester, M. Aspelmeyer, L. Novotny, R. Quidant, and O. Romero-Isart, *Levitodynamics: Levitation and control of microscopic objects in vacuum*, *Science* **374**, 6564 (2021).
- [32] C. Whittle, E. D. Hall, S. Dwyer, N. Mavalvala, V. Sudhir, R. Abbott, A. Ananyeva, C. Austin, L. Barsotti, J. Betzwieser et al., *Approaching the motional ground state of a 10-kg object*, *Science* **372**, 1333 (2021).
- [33] J. Gieseler, B. Deutsch, R. Quidant, and L. Novotny, *Subkelvin Parametric Feedback Cooling of a Laser-Trapped Nanoparticle*, *Phys. Rev. Lett.* **109**, 103603 (2012).
- [34] A. C. Doherty, and K. Jacobs, *Feedback control of quantum systems using continuous state estimation*, *Phys. Rev. A* **60**, 2700 (1999).
- [35] L. S. Walker, G. R. M. Robb, and A. J. Daley, *Measurement and feedback for cooling heavy levitated particles in low-frequency traps*, *Phys. Rev. A* **100**, 063819 (2019).
- [36] A. Vinante, A. Pontin, M. Rashid, M. Toroš, P. F. Barker, and H. Ulbricht, *Testing collapse models with levitated nanoparticles: Detection challenge*, *Phys. Rev. A* **100**, 012119 (2019).
- [37] L. Magrini, P. Rosenzweig, C. Bach, A. Deutschmann-Olek, S. G. Hofer, S. Hong, N. Kiesel, A. Kugi, and M. Aspelmeyer, *Real-time optimal quantum control of mechanical motion at room temperature*, *Nature* **595**, 373 (2021).
- [38] F. Tebbenjohanns, M. Luisa Mattana, M. Rossi, M. Frimmer, and L. Novotny, *Quantum control of a nanoparticle optically levitated in cryogenic free space*, *Nature* **595**, 378 (2021).
- [39] K. Jacobs, *Quantum measurement theory and its applications*, Cambridge University Press (2014).
- [40] H. M. Wiseman, and G. J. Milburn, *Quantum measurement and control*. Cambridge University Press (2009).
- [41] Y. Leng, R. Li, X. Kong, H. Xie, D. Zheng, P. Yin, F. Xiong, T. Wu, C.-K. Duan, Y. Du, Z. Yin, P. Huang, and J. Du, *Mechanical Dissipation Below 1 μ Hz with a Cryogenic Diamagnetic Levitated Micro-Oscillator*, *Phys. Rev. Applied* **15**, 024061 (2021).
- [42] J. Vovrosh, M. Rashid, D. Hempston, J. Bateman, M. Paternostro,

- tro, and H. Ulbricht, *Parametric feedback cooling of levitated optomechanics in a parabolic mirror trap*, *J. Opt. Soc. Am. B* **34**, 1421 (2017).
- [43] R. W. Taylor, and V. Sandoghdar, *Interferometric scattering microscopy: seeing single nanoparticles and molecules via Rayleigh scattering*, *Nano letters* **19**, 4827 (2019).
- [44] G. Cerchiari, L. Dania, D. S. Bykov, R. Blatt, and T. E. Northup, *Position measurement of a dipolar scatterer via self-homodyne detection*, *Phys. Rev. A* **104**, 053523 (2021).
- [45] C. Mawby, and J. J. Halliwell, *Leggett-Garg violations for continuous variable systems with gaussian states*, upcoming arXiv post.

Appendix A: Deriving the form of two-time Leggett-Garg inequality used in this paper

We consider the experimental scenario relevant to the treatment given in this paper where an observable Q is measured at the instant $t = t_1$ and another observable R is measured at $t = t_2$, where $t_1 < t_2$. Here, the measured values of Q and R can be $+1$ or -1 depending on the state of the system.

Now, ‘realism’ implies that Q and R can each be assigned a value ± 1 at any instant, independent of measurement. Let $v(Q)$ and $v(R)$ be such values assigned to Q at instant $t = t_1$ and R at $t = t_2$ respectively. Since $v(Q) = \pm 1$, $v(R) = \pm 1$, we have for $s_1 = \pm 1$ and $s_2 = \pm 1$ that

$$(1 + s_1 v(Q))(1 + s_2 v(R)) = 0 \text{ or } 4. \quad (\text{A1})$$

Hence, the above expression leads to the following,

$$1 + s_1 \langle Q \rangle_G + s_2 \langle R \rangle_G + s_1 s_2 \langle QR \rangle_G \geq 0, \quad (\text{A2})$$

where $\langle \dots \rangle_G$ denotes the average over a grand ensemble, where the two observables Q and R are measured at instants $t = t_1$ and $t = t_2$ respectively.

Next, using the assumption of noninvasive measurability, we obtain

$$\langle R \rangle_{\overline{Q}} = \langle R \rangle_G, \quad (\text{A3})$$

where $\langle \dots \rangle_{\overline{Q}}$ is an average over an ensemble identical to the above-mentioned grand ensemble, with the exception that the observable Q is not measured.

Hence, from Eqs.(A2) and (A3) we get the following modified two-time LGI,

$$1 + s_1 \langle Q \rangle_G + s_2 \langle R \rangle_{\overline{Q}} + s_1 s_2 \langle QR \rangle_G \geq 0. \quad (\text{A4})$$

Appendix B: Deriving the observable probabilities for the time-evolving Schrödinger coherent state of a linear harmonic oscillator

Consider the following initial Gaussian wave function peaked at $x = 0$ at instant $t = 0$,

$$\psi(x, t = 0) = N_s \exp\left(-\frac{x^2}{4\sigma_0^2} + \frac{ip_0 x}{\hbar}\right)$$

$$\text{with } N_s = \sqrt{\frac{1}{\sqrt{2\pi}\sigma_0}} \quad (\text{B1})$$

with the initial momentum expectation value p_0 , and the width $\sigma_0 = \sqrt{\hbar/(2m\omega)}$, where ω is the angular frequency of oscillation and m is the mass.

The state evolved under the linear harmonic potential from instant $t = t_i$ to $t = t_j$ (with $t_j - t_i = \Delta_t$) can be evaluated using the following propagator,

$$K(x', t = t_i; x, t = t_j) = N_p \exp\left[\frac{im\omega}{2\hbar \sin \omega \Delta_t} \{(x^2 + x'^2) \cos \omega \Delta_t - 2xx'\}\right]$$

$$\text{with } N_p = \sqrt{\frac{m\omega}{2\pi i \hbar \sin \omega \Delta_t}} \quad (\text{B2})$$

At the instant $t = t_1 = 0$, we perform the dichotomic measurement of the observable Q that determines whether the oscillating particle is in the state 1 (in between $x = \beta_1$ and $x \rightarrow -\infty$), or in the state 2 (in between $x = \beta_1$ and $x \rightarrow +\infty$). Here β_1 is a real number. The outcomes -1 and $+1$ correspond to finding the particle in the state 1 and in the state 2 respectively.

At the instant $t = t_2$, we perform another dichotomic measurement of the observable R that determines whether the oscillating particle is in the state 3 (in between $x = \beta_2$ and $x \rightarrow -\infty$), or in the state 4 (in between $x = \beta_2$ and $x \rightarrow +\infty$). Here, β_2 is a real number. The outcomes -1 and $+1$ correspond to finding the particle in the state 3 and in the state 4 respectively.

Let us choose $\beta_1 = 0$. Depending on the outcomes -1 and $+1$ of the above-mentioned measurement at the instant $t = t_1 = 0$, the post-measurement states (not normalized) are given by,

$$\begin{aligned} |\psi(t=0)\rangle_- &= \int_{-\infty}^0 dx \psi(x, t=0)|x\rangle, \\ |\psi(t=0)\rangle_+ &= \int_0^{\infty} dx \psi(x, t=0)|x\rangle, \end{aligned} \quad (\text{B3})$$

Hence, the time-evolved unnormalized wave function at the instant $t = t_2$, when the outcome -1 is obtained at $t = 0$, is given by,

$$\begin{aligned} \psi_-(x, t = t_2) &= \int_{-\infty}^0 K(x', t = 0; x, t = t_2) \psi(x', t = 0) dx' \\ &= N_s N_p \exp\left(\frac{im\omega x^2 \cos(\omega t_2)}{2\hbar \sin(\omega t_2)}\right) \int_{-\infty}^0 dx' \exp(-ax'^2 + ibx') \end{aligned} \quad (\text{B4})$$

with

$$\begin{aligned} a &= \frac{1}{4\sigma_0^2} - \frac{im\omega \cos(\omega t_2)}{2\hbar \sin(\omega t_2)}, \\ b &= \frac{p_0}{\hbar} - \frac{m\omega x}{\hbar \sin(\omega t_2)}. \end{aligned}$$

Similarly, the time-evolved unnormalized wave function at the instant $t = t_2$, when the outcome $+1$ is obtained at $t = 0$, is given by,

$$\begin{aligned} \psi_+(x, t = t_2) &= \int_0^{\infty} K(x', t = 0; x, t = t_2) \psi(x', t = 0) dx' \\ &= N_s N_p \exp\left(\frac{im\omega x^2 \cos(\omega t_2)}{2\hbar \sin(\omega t_2)}\right) \int_0^{\infty} dx' \exp(-ax'^2 + ibx') \end{aligned} \quad (\text{B5})$$

Now, it can be checked that

$$\begin{aligned} \int_{-\infty}^0 dx' \exp(-ax'^2 + ibx') &= \frac{\sqrt{\pi}}{2\sqrt{a}} \exp\left(-\frac{b^2}{4a}\right) \left[1 - \operatorname{erf}\left(\frac{ib}{2\sqrt{a}}\right)\right], \\ \int_0^{\infty} dx' \exp(-ax'^2 + ibx') &= \frac{\sqrt{\pi}}{2\sqrt{a}} \exp\left(-\frac{b^2}{4a}\right) \left[1 + \operatorname{erf}\left(\frac{ib}{2\sqrt{a}}\right)\right], \end{aligned} \quad (\text{B6})$$

where the error function $\operatorname{erf}(z) = (2/\sqrt{\pi}) \int_0^z dt \exp(-t^2)$.

Hence, we have

$$\psi_{\pm}(x, t = t_2) = N_s N_p \exp\left(\frac{im\omega x^2 \cos(\omega t_2)}{2\hbar \sin(\omega t_2)}\right) \frac{\sqrt{\pi}}{2\sqrt{a}} \exp\left(-\frac{b^2}{4a}\right) \left[1 \pm \operatorname{erf}\left(\frac{ib}{2\sqrt{a}}\right)\right]. \quad (\text{B7})$$

We, therefore, have the following forms of joint probabilities

$$\begin{aligned} p(Q_{\pm}, R-) &= |N_s|^2 |N_p|^2 \frac{\pi}{4|a|} \int_{-\infty}^{\beta_2} dx \left| \exp\left(-\frac{b^2}{4a}\right) \right|^2 \left| 1 \pm \operatorname{erf}\left(\frac{ib}{2\sqrt{a}}\right) \right|^2, \\ &= \frac{\sqrt{\frac{m\omega}{\hbar}}}{4\sqrt{\pi}} \int_{-\infty}^{\beta_2} dx \exp\left[-\left(x\sqrt{\frac{m\omega}{\hbar}} - \frac{p_0 \sin(\omega t_2)}{\sqrt{\hbar m\omega}}\right)^2\right] \left| 1 \pm \operatorname{erf}\left[\frac{i\left(\frac{p_0 \sin(\omega t_2)}{\sqrt{\hbar m\omega}} - x\sqrt{\frac{m\omega}{\hbar}}\right)}{\sin(\omega t_2)\sqrt{2 - 2i \cot(\omega t_2)}}\right] \right|^2, \end{aligned} \quad (\text{B8})$$

and

$$p(Q_{\pm}, R+) = |N_s|^2 |N_p|^2 \frac{\pi}{4|a|} \int_{\beta_2}^{\infty} dx \left| \exp\left(-\frac{b^2}{4a}\right) \right|^2 \left| 1 \pm \operatorname{erf}\left(\frac{ib}{2\sqrt{a}}\right) \right|^2,$$

$$= \frac{\sqrt{\frac{m\omega}{\hbar}}}{4\sqrt{\pi}} \int_{\beta_2}^{\infty} dx \exp \left[- \left(x \sqrt{\frac{m\omega}{\hbar}} - \frac{p_0 \sin(\omega t_2)}{\sqrt{\hbar m \omega}} \right)^2 \right] \left| 1 \pm \operatorname{erf} \left[\frac{i \left(\frac{p_0 \sin(\omega t_2)}{\sqrt{\hbar m \omega}} - x \sqrt{\frac{m\omega}{\hbar}} \right)}{\sin(\omega t_2) \sqrt{2} - 2i \cot(\omega t_2)} \right] \right|^2. \quad (\text{B9})$$

Now, we perform the following change of variable: $y = x \sqrt{\frac{m\omega}{\hbar}} - \frac{p_0 \sin(\omega t_2)}{\sqrt{\hbar m \omega}}$. With this, the expressions for the above-mentioned joint probabilities become

$$p(Q\pm, R-) = \frac{1}{4\sqrt{\pi}} \int_{-\infty}^{\gamma} dy \exp[-y^2] \left| 1 \pm \operatorname{erf} \left[\frac{-iy}{\sin(\omega t_2) \sqrt{2} - 2i \cot(\omega t_2)} \right] \right|^2,$$

$$p(Q\pm, R+) = \frac{1}{4\sqrt{\pi}} \int_{\gamma}^{\infty} dy \exp[-y^2] \left| 1 \pm \operatorname{erf} \left[\frac{-iy}{\sin(\omega t_2) \sqrt{2} - 2i \cot(\omega t_2)} \right] \right|^2, \quad \text{with } \gamma = \beta_2 \sqrt{\frac{m\omega}{\hbar}} - \frac{p_0 \sin(\omega t_2)}{\sqrt{\hbar m \omega}}. \quad (\text{B10})$$

Now, let us evaluate the probabilities $p(Q\pm)$. It can easily be checked that

$$p(Q-) = \int_{-\infty}^0 |\psi(x, t=0)|^2 = \frac{1}{2}, \quad (\text{B11})$$

and

$$p(Q+) = \int_0^{\infty} |\psi(x, t=0)|^2 = \frac{1}{2}. \quad (\text{B12})$$

Next, let us evaluate the probabilities $p(R\pm)$. For this, consider that no measurement is performed at $t = t_1 = 0$. Under this condition, the time-evolved wave function at the instant $t = t_2$ is given by,

$$\begin{aligned} \psi(x, t = t_2) &= \int_{-\infty}^{\infty} K(x', t = 0; x, t = t_2) \psi(x', t = 0) dx' \\ &= N_s N_p \exp \left(\frac{i m \omega x^2 \cos(\omega t_2)}{2 \hbar \sin(\omega t_2)} \right) \int_{-\infty}^{\infty} dx' \exp(-ax'^2 + ibx') \end{aligned} \quad (\text{B13})$$

with

$$\begin{aligned} a &= \frac{1}{4\sigma_0^2} - \frac{i m \omega \cos(\omega t_2)}{2 \hbar \sin(\omega t_2)}, \\ b &= \frac{p_0}{\hbar} - \frac{m \omega x}{\hbar \sin(\omega t_2)}. \end{aligned}$$

It can be checked that

$$\int_{-\infty}^{\infty} dx' \exp(-ax'^2 + ibx') = \frac{\sqrt{\pi}}{\sqrt{a}} \exp\left(-\frac{b^2}{4a}\right). \quad (\text{B14})$$

Using the above integral, we have

$$\psi(x, t = t_2) = N_s N_p \exp \left(\frac{i m \omega x^2 \cos(\omega t_2)}{2 \hbar \sin(\omega t_2)} \right) \frac{\sqrt{\pi}}{\sqrt{a}} \exp\left(-\frac{b^2}{4a}\right). \quad (\text{B15})$$

Hence, we have the following forms of probabilities

$$\begin{aligned} P(R-) &= |N_s|^2 |N_p|^2 \frac{\pi}{|a|} \int_{-\infty}^{\beta_2} dx \left| \exp\left(-\frac{b^2}{4a}\right) \right|^2 \\ &= \frac{1}{2} \left[1 + \operatorname{erf} \left(\frac{\beta_2 m \omega - p_0 \sin(\omega t_2)}{\sqrt{\hbar m \omega}} \right) \right], \\ &= \frac{1}{2} [1 + \operatorname{erf}(\gamma)], \end{aligned}$$

Probability Densities

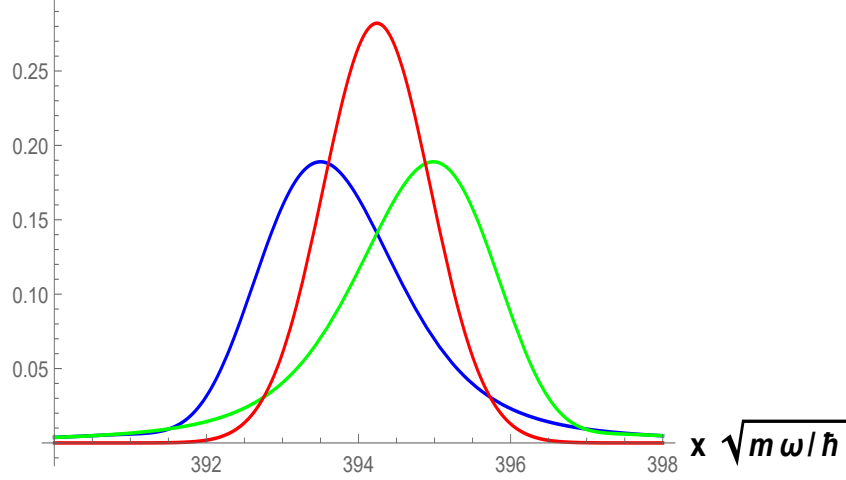


FIG. 1: The blue, green and red curves denote the plots of $|\psi_-(x, t = t_2)|^2$, $|\psi_+(x, t = t_2)|^2$, $|\psi(x, t = t_2)|^2$ versus $\tilde{x} = x \sqrt{\frac{m\omega}{\hbar}}$ respectively for $m = 10^{20}$ amu, $p_0 = 3.3 \times 10^{-15}$ kg m/s, $\omega = 2 \times 10^6$ Hz, $t_2 = T/8$. Here we have shown the plots near $\tilde{x}_0^{(t_2)} = x_0^{(t_2)} \sqrt{\frac{m\omega}{\hbar}}$ with $x_0^{(t_2)} = p_0 \sin(\omega t_2)/(m\omega)$. In other regions, $|\psi_-(x, t = t_2)|^2$, $|\psi_+(x, t = t_2)|^2$, $|\psi(z, t = t_2)|^2$ become vanishingly small.

$$\begin{aligned}
 P(R+) &= |N_s|^2 |N_p|^2 \frac{\pi}{2|a|} \int_{\beta_2}^{\infty} dx \left| \exp\left(-\frac{b^2}{4a}\right) \right|^2 \\
 &= \frac{1}{2} \left[1 - \operatorname{erf}\left(\frac{\beta_2 m\omega - p_0 \sin(\omega t_2)}{\sqrt{\hbar m\omega}}\right) \right], \\
 &= \frac{1}{2} [1 - \operatorname{erf}(\gamma)], \quad \text{with } \gamma = \beta_2 \sqrt{\frac{m\omega}{\hbar}} - \frac{p_0 \sin(\omega t_2)}{\sqrt{\hbar m\omega}}.
 \end{aligned} \tag{B16}$$

Appendix C: Choosing the boundary $x = \beta_2$ between two regions in case of the second measurement at $t = t_2$

If the QM description of the dynamical evolution of the coherent state of linear harmonic oscillator satisfies the assumptions of MR (predefined values of Q are revealed by measurements at the initial instant $t = t_1$ which do not affect the subsequent time evolution of the state), then the following condition must hold good: The QM position probability density at the subsequent instant $t = t_2$ without any measurement performed at $t = t_1$ needs to be equal to the weighted sum of the time evolved probability densities at $t = t_2$ corresponding to the respective outcomes ± 1 obtained by measuring Q at $t = t_1$, mathematically expressed as follows,

$$|\psi(x, t = t_2)|^2 = p_+ |\psi_+(x, t = t_2)|^2 + p_- |\psi_-(x, t = t_2)|^2, \tag{C1}$$

where $\psi(x, t = t_2)$ is the wave function at $t = t_2$ without any measurement at $t = t_1$; $\psi_{\pm}(x, t = t_2)$ are the normalized wave functions at $t = t_2$ when the outcomes ± 1 are obtained by performing the measurement of Q at $t = t_1$; p_+ and p_- are the probabilities with which the values $+1$ and -1 , respectively, are assigned to the observable Q at $t = t_1$. Also, MR implies p_{\pm} should be equal to the observable probabilities $p(Q_{\pm}) = 1/2$. Any deviation from the condition (C1) will signify quantum violation of MR.

Next, let us investigate the nature of $|\psi(x, t = t_2)|^2$ and $|\psi_{\pm}(x, t = t_2)|^2$ in the present context to assess a priori the location of the boundary for the second measurement (at $x = \beta_2$) most favorable for showing QM violation of Eq.(C1).

First, note that the expression of $|\psi(x, t = t_2)|^2$ is given by,

$$|\psi(x, t = t_2)|^2 = \frac{\sqrt{\frac{m\omega}{\hbar}}}{\sqrt{\pi}} \exp \left[- \left(\frac{x - \frac{p_0 \sin(\omega t_2)}{m\omega}}{\sqrt{\frac{\hbar}{m\omega}}} \right)^2 \right]. \tag{C2}$$

Hence, this is a Gaussian distribution with peak at $x_0^{(t_2)} = p_0 \sin(\omega t_2)/(m\omega)$ and standard deviation $\Delta^{(t_2)} = \sqrt{\hbar/(2m\omega)}$.

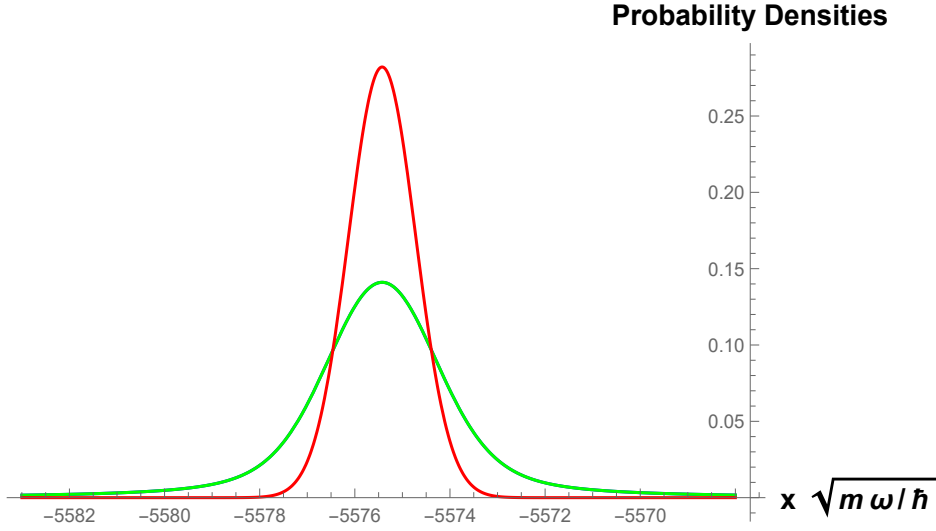


FIG. 2: The green curve denotes the plot of both $|\psi_-(x, t = t_2)|^2$ and $|\psi_+(x, t = t_2)|^2$ versus $\tilde{x} = x \sqrt{\frac{m\omega}{\hbar}}$. On the other hand, the red curve denotes the plot of $|\psi(x, t = t_2)|^2$ versus $\tilde{x} = x \sqrt{\frac{m\omega}{\hbar}}$ for $m = 10^6$ amu, $p_0 = 3.3 \times 10^{-21}$ kg m/s, $\omega = 2 \times 10^6$ Hz, $t_2 = 3T/4$. Here we have shown the plots near $\tilde{x}_0^{(t_2)} = x_0^{(t_2)} \sqrt{\frac{m\omega}{\hbar}}$ with $x_0^{(t_2)} = p_0 \sin(\omega t_2)/(m\omega)$. In other regions, $|\psi_-(x, t = t_2)|^2$, $|\psi_+(x, t = t_2)|^2$, $|\psi(x, t = t_2)|^2$ become vanishingly small.

Next, the expressions of $|\psi_{\pm}(x, t = t_2)|^2$ are given by,

$$|\psi_{\pm}(x, t = t_2)|^2 = \frac{\sqrt{\frac{m\omega}{\hbar}}}{4\sqrt{\pi}} \exp \left[- \left(\frac{x - \frac{p_0 \sin(\omega t_2)}{m\omega}}{\sqrt{\frac{\hbar}{m\omega}}} \right)^2 \right] \left| 1 \pm \operatorname{erf} \left[\frac{-i \left(x - \frac{p_0 \sin(\omega t_2)}{m\omega} \right)}{\sqrt{\frac{\hbar}{m\omega}} \sin(\omega t_2) \sqrt{2 - 2i \cot(\omega t_2)}} \right] \right|^2. \quad (\text{C3})$$

Now, for some choices of t_2 , these are Gaussian-like distributions with the peaks being slightly shifted from $x_0^{(t_2)} = p_0 \sin(\omega t_2)/(m\omega)$. For example, let us take $m = 10^{20}$ amu, $p_0 = 3.3 \times 10^{-15}$ kg m/s, $\omega = 2 \times 10^6$ Hz, $t_2 = T/8$, where $T = 2\pi/\omega$ is the time-period. For this choice of the parameters, the plots of $|\psi_{\pm}(x, t = t_2)|^2$ and $|\psi(x, t = t_2)|^2$ are presented in Fig. 1.

Also, for some choices of t_2 , $|\psi_{\pm}(x, t = t_2)|^2$ given by Eq.(C3) are Gaussian-like distributions with the peaks being situated at $x_0^{(t_2)} = p_0 \sin(\omega t_2)/(m\omega)$, but slightly broadened compared to $|\psi(x, t = t_2)|^2$. For example, let us take $m = 10^6$ amu, $p_0 = 3.3 \times 10^{-21}$ kg m/s, $\omega = 2 \times 10^6$ Hz, $t_2 = 3T/4$, where $T = 2\pi/\omega$ is the time-period. For this choice of the parameters, the plots of $|\psi(x, t = t_2)|^2$ and $|\psi_{\pm}(x, t = t_2)|^2$ are presented in Fig. 2.

The plots of $|\psi_{\pm}(x, t = t_2)|^2$ and $|\psi(x, t = t_2)|^2$ are of similar natures for other different choices of parameters.

From these two plots, we observe the following features:

- All the distributions $|\psi(x, t = t_2)|^2$ and $|\psi_{\pm}(x, t = t_2)|^2$ become vanishingly small at x far away from $x_0^{(t_2)}$.
- The difference between $|\psi(x, t = t_2)|^2$ and $(1/2)(|\psi_+(x, t = t_2)|^2 + |\psi_-(x, t = t_2)|^2)$ can be seen at $x = x_0^{(t_2)} \pm c\Delta^{(t_2)}$ with c being a positive number, and c being of the order of 10^{-1} or 1.

Before proceeding further, it is useful to note that the measurement statistics of R at $t = t_2$ is determined from the area under the curve $|\psi(x, t = t_2)|^2$ or $|\psi_+(x, t = t_2)|^2$ or $|\psi_-(x, t = t_2)|^2$ in the region from $x = \beta_2$ to $x = \infty$ or from $x = -\infty$ to $x = \beta_2$. In particular, $p(R+)$ and $p(R-)$ are nothing but the areas under the curve $|\psi(x, t = t_2)|^2$ in the region from $x = \beta_2$ to $x = \infty$ and from $x = -\infty$ to $x = \beta_2$ respectively. On the other hand, $p(Q\pm, R+)$ and $p(Q\pm, R-)$ are the areas under the curve $|\psi_{\pm}(x, t = t_2)|^2$ in the region from $x = \beta_2$ to $x = \infty$ and from $x = -\infty$ to $x = \beta_2$ respectively.

Now, it is seen from Figs. 1 and 2 that the difference between the areas under the curves $|\psi(x, t = t_2)|^2$ and $(1/2)(|\psi_+(x, t = t_2)|^2 + |\psi_-(x, t = t_2)|^2)$ in any of the two measurement regions (either from $x = \beta_2$ to $x = \infty$ or from $x = -\infty$ to $x = \beta_2$) vanishes if β_2 is chosen far away from the region $x_0^{(t_2)} \pm c\Delta^{(t_2)}$ with $c > 0$ being of the order of 10^{-1} or 1. There will be difference between the areas under the curves- $|\psi(x, t = t_2)|^2$ and $(1/2)(|\psi_+(x, t = t_2)|^2 + |\psi_-(x, t = t_2)|^2)$ in any of the aforementioned two regions only if β_2 is chosen at $x = x_0^{(t_2)} \pm c\Delta^{(t_2)}$. Also, if β_2 is chosen at $x_0^{(t_2)}$, then there is no difference between the areas the curves- $|\psi(x, t = t_2)|^2$ and $(1/2)(|\psi_+(x, t = t_2)|^2 + |\psi_-(x, t = t_2)|^2)$ in the region

from $x = \beta_2$ to $x = \infty$ or in the region from $x = -\infty$ to $x = \beta_2$. Hence, the difference between $|\psi(x, t = t_2)|^2$ and $(1/2)(|\psi_+(x, t = t_2)|^2 + |\psi_-(x, t = t_2)|^2)$ is likely to be reflected in the measurement statistics of Q and R if β_2 is chosen at $x = x_0^{(t_2)} \pm c\Delta^{(t_2)}$.

Based on the above consideration, for the purpose of our analysis, we have therefore chosen the boundary between the two measurement regions for the second measurement at $t = t_2$ to be located at $x = \beta_2 = x_0^{(t_2)} \pm c\Delta^{(t_2)}$ with $c > 0$ being of the order of 10^{-1} or 1.

Appendix D: Details on the practical challenges with large mass

In practical situations, it is almost impossible to keep the boundary between the two regions (illuminated and unilluminated) to be fixed in all experimental runs. Rather, we can expect that the aforementioned boundary at $t = t_i$ will be at $\beta_i + \epsilon_i$ (where ϵ_i is a small positive/negative number), where ϵ_i will be different in different runs. In effect, the observed violation of the two-time NSIT will be the statistical average of different (positive or negative) values of N_+ , N_- corresponding to different ϵ_1 and ϵ_2 . Similarly, the observed violation of the two-time LGI will be the statistical average of different (positive or negative) values of $L_{+,+}$, $L_{+,-}$, $L_{-,+}$, $L_{-,-}$ corresponding to different ϵ_1 and ϵ_2 .

Let us, at first, determine the quantum violation of two-time NSIT/LGI with the boundary between the two regions in case of first measurement being located at $x = \beta_1 + \epsilon_1$ and that in case of second measurement being located at $x = \beta_2 + \epsilon_2$, where ϵ_1 and ϵ_2 are two fixed positive or negative numbers.

The first measurement of Q at $t = t_1 = 0$ determines whether the particle is in the region from $x = -\infty$ to $x = \beta_1 + \epsilon_1$ (corresponds to the outcome -1), or from $x = \beta_1 + \epsilon_1$ to $x = \infty$ (corresponds to the outcome $+1$), where $\beta_1 = 0$ and ϵ_1 can be positive or negative. Depending on the outcomes -1 and $+1$ of this measurement, the post-measurement states (not normalized) are given by,

$$\begin{aligned} |\psi(t=0)\rangle_- &= \int_{-\infty}^{\epsilon_1} dx \psi(x, t=0)|x\rangle, \\ |\psi(t=0)\rangle_+ &= \int_{\epsilon_1}^{\infty} dx \psi(x, t=0)|x\rangle, \end{aligned} \quad (D1)$$

Hence, the time-evolved unnormalized wave function at the instant $t = t_2$, when the outcome -1 is obtained at $t = 0$, is given by,

$$\begin{aligned} \psi_-(x, t = t_2) &= \int_{-\infty}^{\epsilon_1} K(x', t = 0; x, t = t_2) \psi(x', t = 0) dx' \\ &= N_s N_p \exp\left(\frac{im\omega x^2 \cos(\omega t_2)}{2\hbar \sin(\omega t_2)}\right) \int_{-\infty}^{\epsilon_1} dx' \exp(-ax'^2 + ibx') \end{aligned} \quad (D2)$$

with

$$\begin{aligned} a &= \frac{1}{4\sigma_0^2} - \frac{im\omega \cos(\omega t_2)}{2\hbar \sin(\omega t_2)}, \\ b &= \frac{p_0}{\hbar} - \frac{m\omega x}{\hbar \sin(\omega t_2)}. \end{aligned}$$

Similarly, the time-evolved unnormalized wave function at the instant $t = t_2$, when the outcome $+1$ is obtained at $t = 0$, is given by,

$$\begin{aligned} \psi_+(x, t = t_2) &= \int_{\epsilon_1}^{\infty} K(x', t = 0; x, t = t_2) \psi(x', t = 0) dx' \\ &= N_s N_p \exp\left(\frac{im\omega x^2 \cos(\omega t_2)}{2\hbar \sin(\omega t_2)}\right) \int_{\epsilon_1}^{\infty} dx' \exp(-ax'^2 + ibx') \end{aligned} \quad (D3)$$

It can be checked that

$$\begin{aligned} \int_{-\infty}^{\epsilon_1} dx' \exp(-ax'^2 + ibx') &= \frac{\sqrt{\pi}}{2\sqrt{a}} \exp\left(-\frac{b^2}{4a}\right) \left[1 - \operatorname{erf}\left(\frac{i(b + 2ia\epsilon_1)}{2\sqrt{a}}\right)\right], \\ \int_{\epsilon_1}^{\infty} dx' \exp(-ax'^2 + ibx') &= \frac{\sqrt{\pi}}{2\sqrt{a}} \exp\left(-\frac{b^2}{4a}\right) \left[1 + \operatorname{erf}\left(\frac{i(b + 2ia\epsilon_1)}{2\sqrt{a}}\right)\right]. \end{aligned} \quad (D4)$$

We, therefore, have the following,

$$\psi_{\pm}(x, t = t_2) = N_s N_p \exp\left(\frac{i m \omega x^2 \cos(\omega t_2)}{2 \hbar \sin(\omega t_2)}\right) \frac{\sqrt{\pi}}{2 \sqrt{a}} \exp\left(-\frac{b^2}{4a}\right) \left[1 \pm \operatorname{erf}\left(\frac{i(b + 2ia\epsilon_1)}{2\sqrt{a}}\right)\right]. \quad (\text{D5})$$

Next, let us also consider that the second measurement of R at $t = t_2$ determines whether the particle is in the region from $x = -\infty$ to $x = \beta_2 + \epsilon_2$ (corresponds to the outcome -1), or from $x = \beta_2 + \epsilon_2$ to $x = \infty$ (corresponds to the outcome $+1$), where $\beta_2 = p_0 \sin(\omega t_2)/(m\omega) + \sqrt{\hbar/(m\omega)}$ as mentioned in the main paper and ϵ_2 is a real number. Hence, we have the following expressions of joint probabilities,

$$\begin{aligned} p(Q_{\pm}, R-) &= |N_s|^2 |N_p|^2 \frac{\pi}{4|a|} \int_{-\infty}^{\beta_2 + \epsilon_2} dx \left| \exp\left(-\frac{b^2}{4a}\right) \right|^2 \left| 1 \pm \operatorname{erf}\left(\frac{i(b + 2ia\epsilon_1)}{2\sqrt{a}}\right) \right|^2, \\ &= \frac{\sqrt{\frac{m\omega}{\hbar}}}{4\sqrt{\pi}} \int_{-\infty}^{\beta_2 + \epsilon_2} dx \exp\left[-\left(x\sqrt{\frac{m\omega}{\hbar}} - \frac{p_0 \sin(\omega t_2)}{\sqrt{\hbar m \omega}}\right)^2\right] \left| 1 \pm \operatorname{erf}\left[\frac{i\left(\frac{p_0 \sin(\omega t_2)}{\sqrt{\hbar m \omega}} - x\sqrt{\frac{m\omega}{\hbar}} + \epsilon_1\sqrt{\frac{m\omega}{\hbar}} \exp[i\omega t_2]\right)}{\sin(\omega t_2)\sqrt{2 - 2i \cot(\omega t_2)}}\right] \right|^2, \end{aligned} \quad (\text{D6})$$

and

$$\begin{aligned} p(Q_{\pm}, R+) &= |N_s|^2 |N_p|^2 \frac{\pi}{4|a|} \int_{\beta_2 + \epsilon_2}^{\infty} dx \left| \exp\left(-\frac{b^2}{4a}\right) \right|^2 \left| 1 \pm \operatorname{erf}\left(\frac{i(b + 2ia\epsilon_1)}{2\sqrt{a}}\right) \right|^2, \\ &= \frac{\sqrt{\frac{m\omega}{\hbar}}}{4\sqrt{\pi}} \int_{\beta_2 + \epsilon_2}^{\infty} dx \exp\left[-\left(x\sqrt{\frac{m\omega}{\hbar}} - \frac{p_0 \sin(\omega t_2)}{\sqrt{\hbar m \omega}}\right)^2\right] \left| 1 \pm \operatorname{erf}\left[\frac{i\left(\frac{p_0 \sin(\omega t_2)}{\sqrt{\hbar m \omega}} - x\sqrt{\frac{m\omega}{\hbar}} + \epsilon_1\sqrt{\frac{m\omega}{\hbar}} \exp[i\omega t_2]\right)}{\sin(\omega t_2)\sqrt{2 - 2i \cot(\omega t_2)}}\right] \right|^2. \end{aligned} \quad (\text{D7})$$

Now, we perform the following change of variable: $y = x\sqrt{\frac{m\omega}{\hbar}} - \frac{p_0 \sin(\omega t_2)}{\sqrt{\hbar m \omega}}$. Also, let us define the following

$$\tilde{\epsilon}_1 = \epsilon_1 \sqrt{\frac{m\omega}{\hbar}}, \quad \tilde{\epsilon}_2 = \epsilon_2 \sqrt{\frac{m\omega}{\hbar}} \quad (\text{D8})$$

With these, the expressions for the above-mentioned joint probabilities become

$$p(Q_{\pm}, R-) = \frac{1}{4\sqrt{\pi}} \int_{-\infty}^{1 + \tilde{\epsilon}_2} dy \exp[-y^2] \left| 1 \pm \operatorname{erf}\left[\frac{i(-y + \tilde{\epsilon}_1 \exp[i\omega t_2])}{\sin(\omega t_2)\sqrt{2 - 2i \cot(\omega t_2)}}\right] \right|^2. \quad (\text{D9})$$

$$p(Q_{\pm}, R+) = \frac{1}{4\sqrt{\pi}} \int_{1 + \tilde{\epsilon}_2}^{\infty} dy \exp[-y^2] \left| 1 \pm \operatorname{erf}\left[\frac{i(-y + \tilde{\epsilon}_1 \exp[i\omega t_2])}{\sin(\omega t_2)\sqrt{2 - 2i \cot(\omega t_2)}}\right] \right|^2. \quad (\text{D10})$$

Now, let us evaluate the probabilities $p(Q_{\pm})$. It can easily be checked that

$$p(Q-) = \int_{-\infty}^{\epsilon_1} |\psi(x, t = 0)|^2 = \frac{1}{2} [1 + \operatorname{erf}(\tilde{\epsilon}_1)], \quad (\text{D11})$$

$$p(Q+) = \int_{\epsilon_1}^{\infty} |\psi(x, t = 0)|^2 = \frac{1}{2} [1 - \operatorname{erf}(\tilde{\epsilon}_1)]. \quad (\text{D12})$$

Next, we will evaluate the probabilities $p(R_{\pm})$. For this, we consider that no measurement is performed at $t = t_1 = 0$. With this, the time-evolved wave function at the instant $t = t_2$ is given by,

$$\begin{aligned} \psi(x, t = t_2) &= \int_{-\infty}^{\infty} K(x', t = t_1; x, t = t_2) \psi(x', t = t_1) dx' \\ &= N_s N_p \exp\left(\frac{i m \omega x^2 \cos(\omega t_2)}{2 \hbar \sin(\omega t_2)}\right) \int_{-\infty}^{\infty} dx' \exp(-ax'^2 + ibx') \\ &= N_s N_p \exp\left(\frac{i m \omega x^2 \cos(\omega t_2)}{2 \hbar \sin(\omega t_2)}\right) \frac{\sqrt{\pi}}{\sqrt{a}} \exp\left(-\frac{b^2}{4a}\right). \end{aligned} \quad (\text{D13})$$

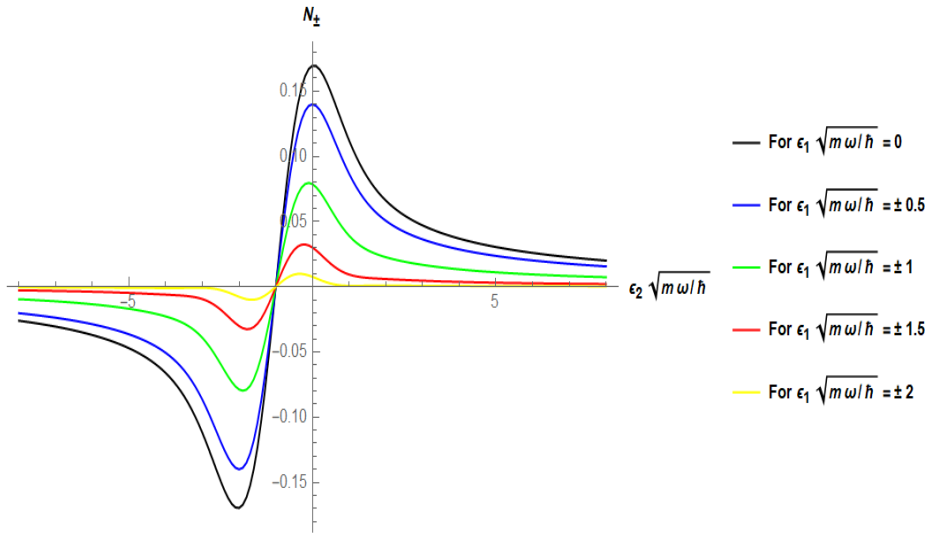


FIG. 3: Plot of quantum violation of the two-time NSIT condition (N_{\pm}) with different choices of $\tilde{\epsilon}_1 = \epsilon_1 \sqrt{m\omega/\hbar}$ versus $\tilde{\epsilon}_2 = \epsilon_2 \sqrt{m\omega/\hbar}$ for $t_2 = T/4$ and for any choice of m, ω, p_0 .

with

$$a = \frac{1}{4\sigma_0^2} - \frac{i m \omega \cos(\omega t_2)}{2\hbar \sin(\omega t_2)},$$

$$b = \frac{p_0}{\hbar} - \frac{m \omega x}{\hbar \sin(\omega t_2)}.$$

Therefore, we have the following form of probabilities

$$P(R-) = |N_s|^2 |N_p|^2 \frac{\pi}{|a|} \int_{-\infty}^{\beta_2 + \epsilon_2} dx \left| \exp\left(-\frac{b^2}{4a}\right) \right|^2$$

$$= \frac{1}{2} \left[1 + \operatorname{erf}\left(\frac{\beta_2 m \omega + \epsilon_2 m \omega - p_0 \sin(\omega t_2)}{\sqrt{\hbar m \omega}}\right) \right],$$

$$= \frac{1}{2} [1 + \operatorname{erf}(1 + \tilde{\epsilon}_2)], \quad (\text{D14})$$

$$P(R+) = |N_s|^2 |N_p|^2 \frac{\pi}{2|a|} \int_{\beta_2 + \epsilon_2}^{\infty} dx \left| \exp\left(-\frac{b^2}{4a}\right) \right|^2$$

$$= \frac{1}{2} \left[1 - \operatorname{erf}\left(\frac{\beta_2 m \omega + \epsilon_2 m \omega - p_0 \sin(\omega t_2)}{\sqrt{\hbar m \omega}}\right) \right],$$

$$= \frac{1}{2} [1 - \operatorname{erf}(1 + \tilde{\epsilon}_2)]. \quad (\text{D15})$$

Using the expressions mentioned in Eqs.(D9), (D10), (D11), (D12), (D14), (D15), the two-time NSIT condition or the two-time LGI can be tested.

Let us take $t_2 = T/4$ as an example. For this choice of t_2 , we plot N_{\pm} with different choices of $\tilde{\epsilon}_1 = \epsilon_1 \sqrt{m\omega/\hbar}$ versus $\tilde{\epsilon}_2 = \epsilon_2 \sqrt{m\omega/\hbar}$ for any choice of m, ω, p_0 in Fig. 3. It is evident from this figure that the permissible ranges of ϵ_1 and ϵ_2 for which one can get quantum violation of the NSIT condition are proportional to $1/(m\omega)$. It can be checked that this feature persists for other choices of t_2 as well.

As mentioned earlier, in realistic situation, the boundary between the two regions in case of the measurements at $t = t_i$ will be at $x = \beta_i + \epsilon_i$, where ϵ_i will be different in different experimental runs. Precise measurement implies that ϵ_i is zero in each experimental run. On the other hand, with an increase in the imprecision, more non-zero values of ϵ_i around 0 will appear in different runs. In other words, as the measurement imprecision increases, the boundaries between the two regions at $t = t_i$ in different runs will be located at more number of different points around β_i .

Now, the observed quantum violation of the two-time NSIT condition will be the statistical average of different values of N_+ or N_- corresponding to different ϵ_1 and ϵ_2 . Hence, the precision of the two measurements required to get significant quantum

violation of the NSIT condition increases with increasing m for any ω . Moreover, for large m , this demand for increasing precision can be countered by decreasing ω .

In a similar way, it can be shown that the permissible ranges of ϵ_1 and ϵ_2 for which one can get quantum violation of the two-time LGI are proportional to $1/(m\omega)$. Hence, in this case also, the precision of the two measurements required to get significant quantum violation of the two-time LGI increases with increasing values of m for any ω . Also, for large m , this necessity for increasing precision in measurements can be avoided by decreasing the angular frequency ω .